

Misfit strain effect on the thermal expansion coefficient of graphene/MoS₂ van der Waals heterostructures

Run-Sen Zhang and Jin-Wu Jiang*

Shanghai Key Laboratory of Mechanics in Energy Engineering,

Shanghai Institute of Applied Mathematics and Mechanics,

School of Mechanics and Engineering Science,

Shanghai University, Shanghai 200072, People's Republic of China

(Dated: June 29, 2021)

Abstract

Van der Waals heterostructures such as graphene/MoS₂ are promising candidates for plenty of optical or electronic applications, owing to advanced properties inherited from the constitutional atomic layers. Thermal expansion is an important phenomenon to be considered for the thermal stability of the van der Waals heterostructure as temperature commonly rises during the operation of nano devices. In the present work, the thermal expansion coefficient for the graphene/MoS₂ heterostructure is investigated by molecular dynamics simulations, and the effect from the unavoidable misfit strain on the thermal expansion coefficient is revealed. The misfit strain can tune the thermal expansion coefficient by a factor of six, and this effect is quite robust in sense that it is not sensitive to the size or direction of the heterostructure. An analytic formula is derived to directly relate the thermal expansion coefficient to the misfit strain of the heterostructure, which qualitatively agrees with the numerical results although the analytic formula underestimates the misfit strain effect. Further analysis discloses that the misfit strain can efficiently engineer the thermal induced ripples, which serves as the key mechanism for the misfit strain effect on the thermal expansion coefficient. These findings provide valuable information for the thermal stability of van der Waals heterostructures and shall be benefit for practical applications of van der Waals heterostructure based nano devices.

Keywords: Van der Waals Heterostructure, Misfit Strain, Thermal Expansion Coefficient

I. INTRODUCTION

As a promising candidate for the next generation electronics, graphene has attracted lots of attention due to its outstanding thermal, mechanical and electronic properties.¹⁻³ The absence of a finite band gap is a major shortcoming for graphene based devices. Forming van der Waals heterostructures is a very useful method to overcome the disadvantage of each individual layer and to finely tune various properties for 2D materials.^{4,5} The combination of graphene with semiconducting two-dimensional transition metal dichalcogenides has potential applications in the field of high power electronics and novel nanometer scale devices.⁶⁻⁸ In particular, the graphene/MoS₂ van der Waals heterostructure has been suggested to be used in high-performance photo detection,⁹ photo catalytic, molecular sieves, and electrodes.¹⁰⁻¹²

For practical applications of the graphene/MoS₂ van der Waals heterostructure, it is crucial to learn the thermal expansion property of such devices because of the reduced dimensionality and high density of devices in tightly packed structures.^{13,14} The thermal expansion phenomenon is characterized by the thermal expansion coefficient (TEC). The TEC of single layer graphene and single layer MoS₂ have been extensively studied by both numerical simulations¹⁵⁻²⁰ and experiments²¹⁻²⁶. Mounet and Marzari predicted that the TEC of single layer graphene is negative up to 2300 K.¹⁵ Zakharchenko et al. showed that graphene has a negative TEC for temperatures below 900 K.¹⁶ It has been shown that the out-of-plane bending (flexural) mode makes a negative contribution to the TEC, while the in-plane anharmonicity makes positive contribution to the TEC.^{19,27} The competition between these two effects leads to the negative TEC at low temperature and positive TEC at high temperature. Experiments confirmed that the TEC is negative for graphene around room temperature.^{22,28} Different from graphene, the monolayer MoS₂ has positive TEC. For instance, micro-Raman spectroscopy measurement obtained the in-plane TEC of monolayer MoS₂ as $7.6 \pm 0.9 \times 10^{-6} \text{ K}^{-1}$ and $7.4 \pm 0.5 \times 10^{-6} \text{ K}^{-1}$ along different directions.²⁴ The MoS₂ atomic layer has larger bending modulus than graphene, so the negative effect from the flexural mode is weaker, leading to positive TEC in the MoS₂ atomic layer.

As a characteristic structural feature, the constitutional layers in the van der Waals heterostructure usually have different lattice constants, which results in the misfit strain between neighboring atomic layers.²⁹⁻³¹ The misfit strain in van der Waals heterostructures can be

adjusted through various methods, including the substrate,³² the structural design,³³ and the photoelectrochemical etching process.³⁴ It has been shown that the misfit strain can cause direct effects on physical and mechanical properties of the van der Waals heterostructure.³⁵

Although the thermal expansion behavior of graphene and MoS₂ layers have been extensively studied, the TEC for the graphene/MoS₂ van der Waals heterostructure has not been well studied. Particularly, the effect of the characteristic misfit strain on the TEC is still unclear, which will be the focus of the present work.

In this paper, we perform molecular dynamics (MD) simulations to comparatively investigate the TEC for graphene/graphene bilayer, MoS₂/MoS₂ bilayer, and the graphene/MoS₂ heterostructure. We focus on the effect of the misfit strain on the TEC in graphene/MoS₂ heterostructures. We find that the TEC along the misfit strain direction decreases from $6 \times 10^{-6} \text{ K}^{-1}$ to $1 \times 10^{-6} \text{ K}^{-1}$ with misfit strain increasing from -6% to 6%. The misfit strain effect can be qualitatively discussed based on an analytic relation between the TEC and the misfit strain. Furthermore, we find that the thermal induced ripples are effectively tuned by the misfit strain, which can cause strong effects on the TEC of the graphene/MoS₂ heterostructure. The nonlinear effect also plays a role in the misfit strain effect on the TEC.

II. STRUCTURE AND SIMULATION DETAILS

Figure 1 shows the three structures studied in the present work, i.e., graphene/graphene bilayer, MoS₂/MoS₂ bilayer, and graphene/MoS₂ heterostructure. The graphene/graphene bilayer structure is in the AB stacking order, while the MoS₂/MoS₂ structure is in its lowest-energy stacking order. The horizontal x-direction is along the armchair direction while the vertical y-direction is along the zigzag direction. The lengths of graphene and MoS₂ are slightly different in the graphene/MoS₂ heterostructure, resulting in the misfit strain as follows,

$$\epsilon_m = -\frac{l_1 - l_2}{l_1}. \quad (1)$$

where l_1 and l_2 are the length for the two constituting layers. The present work focuses on the effect of the misfit strain ϵ_m on the thermal expansion coefficient of the graphene/MoS₂ heterostructure.

The carbon-carbon interaction is described by the second generation Brenner (REBO-II)

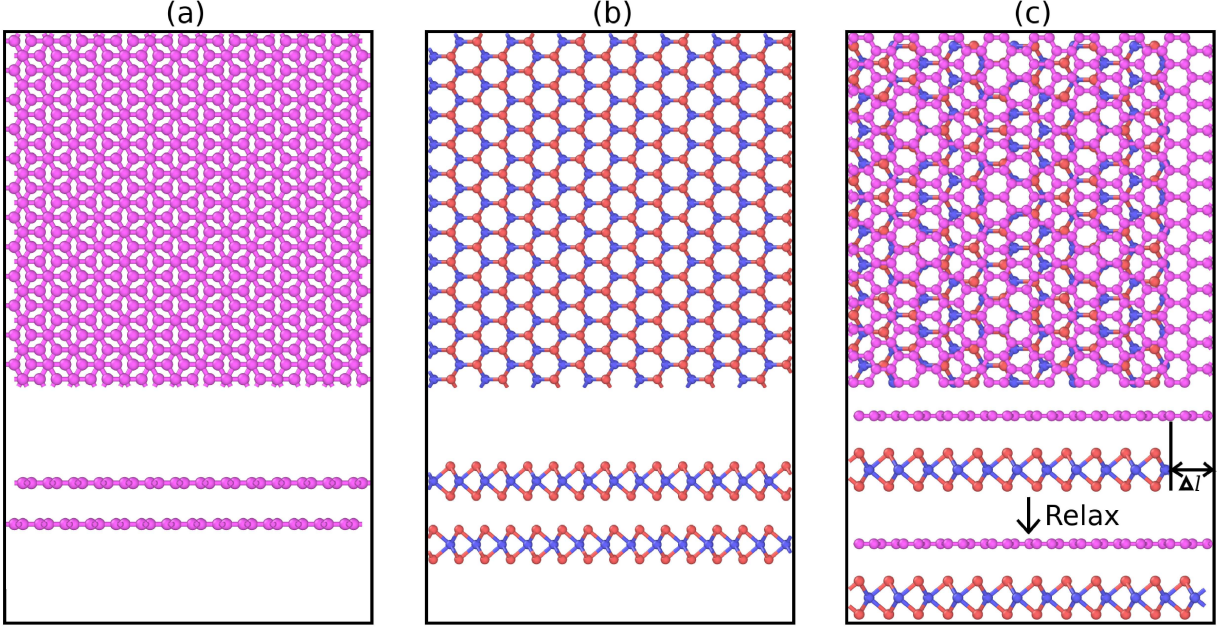


FIG. 1: Bilayer structures studied in the present work. (a) The graphene/graphene structure. (b) The MoS₂/MoS₂ structure. (c) The graphene/MoS₂ heterostructure. The graphene and MoS₂ have a difference of Δl in their length, resulting in the misfit strain in the relaxed configuration of the graphene/MoS₂ heterostructure.

potential,³⁶ while the MoS₂ interatomic interactions are described by the Stillinger-Weber potential³⁷ with parameters from the recent work.³⁸ The inter-layer interactions between graphene/graphene, MoS₂/MoS₂ and graphene/MoS₂ are described by the Lennard-Jones potential. The distance and energy parameters in the Lennard-Jones potential are listed in table I.

TABLE I: Lennard-Jones parameters used in the present work for graphene/graphene,³⁹ MoS₂/MoS₂,³⁹ and graphene/MoS₂.²⁹

structures	ϵ (meV)	σ (Å)	cut off (Å)
graphene/graphene	2.96	3.382	10.0
MoS ₂ /MoS ₂	23.6	3.18	10.0
graphene/MoS ₂	3.95	3.625	10.0

All MD simulations are performed based on the LAMMPS package,⁴⁰ and the OVITO

package is used for visualization.⁴¹ The standard Newton equations of motion are integrated in time using the velocity Verlet algorithm with a time step of 1 fs. Periodic boundary conditions are employed in the two in-plane directions, while the free boundary condition is applied in the out-of-plane direction.

The thermal expansion phenomenon is simulated as follows. Firstly, the structure is minimized to the lowest-energy configuration using the conjugate gradient algorithm and then optimized for 200 ps within the NPT ensemble (i.e. the particles number N , the pressure P and the temperature T of the system are constant) at desired temperatures at zero pressure. Secondly, the structure is allowed to evolve for 1 ns within the NPT ensemble, and the size for the structure is averaged during this step. The averaged size L at different temperature T is then used to compute the thermal expansion coefficient. The standard deviation error ΔL in the time average gives the error bar for the size.

III. RESULTS AND DISCUSSION

A. Simulation results

Figure 2 shows the temperature dependence for the sizes of graphene/graphene and MoS₂/MoS₂ bilayer structures. Panel (a) shows the temperature dependence for the two lateral dimensions for the graphene/graphene structure of dimension about 200×200 Å. The relation between the size and the temperature is fitted to a linear function, with a slope of $\frac{dL}{dT}$. The one-dimensional TEC, α , is calculated by

$$\alpha = \frac{1}{L_0} \frac{dL}{dT}, \quad (2)$$

where L_0 is the size at zero temperature. From Fig.2 (a), the TEC of the graphene/graphene structure is $1.54 \times 10^{-6} \text{ K}^{-1}$ and $1.35 \times 10^{-6} \text{ K}^{-1}$ along the x and y directions, respectively. We also calculate the TEC of monolayer graphene, which is a negative value of $-2.1 \times 10^{-6} \text{ K}^{-1}$ at 400 K. We find that the TEC of the graphene/graphene bilayer structure is larger than the monolayer graphene. It is because the negative TEC in monolayer graphene is mainly caused by the low-frequency flexural mode, which is limited in the graphene/graphene structure with larger bending modulus. Similar layer dependence for the TEC has also been found in previous Monte Carlo works.⁴² The TEC for the MoS₂/MoS₂ structure is $7.63 \times 10^{-6} \text{ K}^{-1}$ along both x and y directions from Fig.2 (b). These value are consistent with the experiment

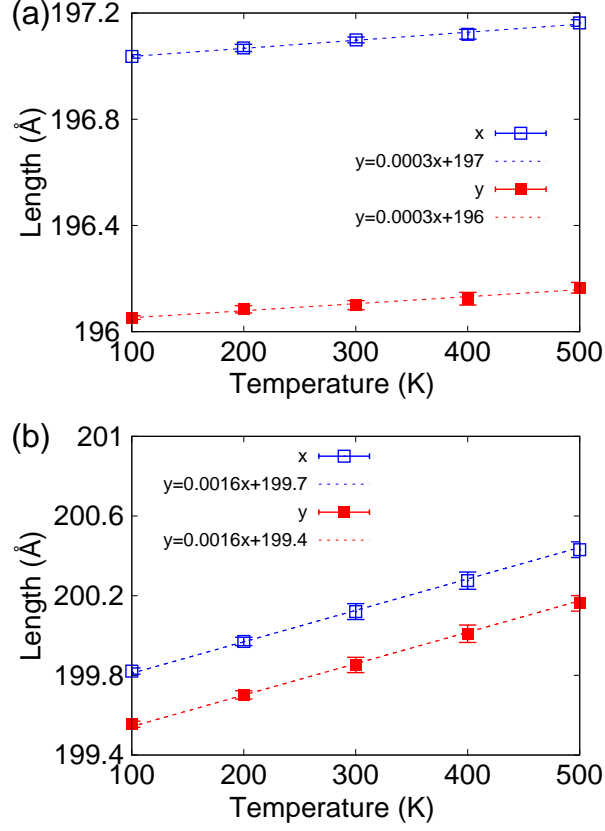


FIG. 2: The temperature dependence for the length of (a) the graphene/graphene structure and (b) the MoS₂/MoS₂ structure.

$(7.6 \pm 0.9 \times 10^{-6} \text{ K}^{-1}$ and $7.4 \pm 0.5 \times 10^{-6} \text{ K}^{-1})^{24}$ and first-principle calculations ($7.3 \times 10^{-6} \text{ K}^{-1}$ and $7.2 \times 10^{-6} \text{ K}^{-1})^{20,43}$. We find that the TEC is almost isotropic in both graphene/graphene and MoS₂/MoS₂ bilayer structures, which is as expected considering the three-fold rotational symmetry in both structures.

Thermal induced ripples are important in two-dimensional materials like the graphene/graphene bilayer structure and the MoS₂/MoS₂ structure. As a result of the ripples, thermal properties in the atomic layers can be size dependent. Indeed, Fig.3 shows that TEC depends on the size for these two bilayer structures. In particular, TEC is obviously larger in smaller structures. All structures simulated in this figure are of square shape with almost the same size in the two lateral dimensions. The size effect can be understood as follows. The height of the thermal induced ripple becomes larger at higher temperature, which consequently decreases the in-plane sizes for the bilayer structures. As a result, the

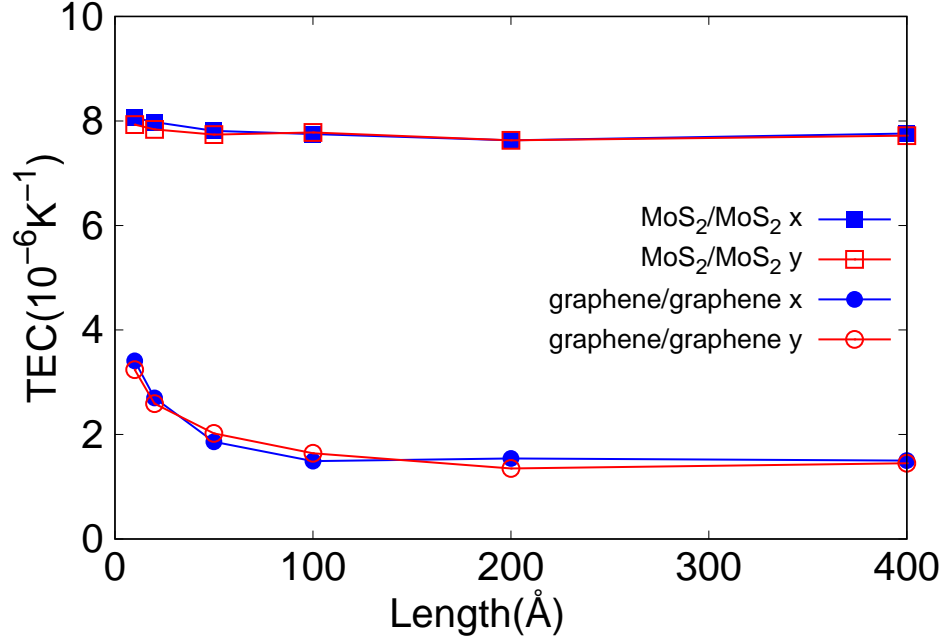


FIG. 3: The size dependence for the TEC of graphene/graphene and MoS₂/MoS₂ structures, respectively.

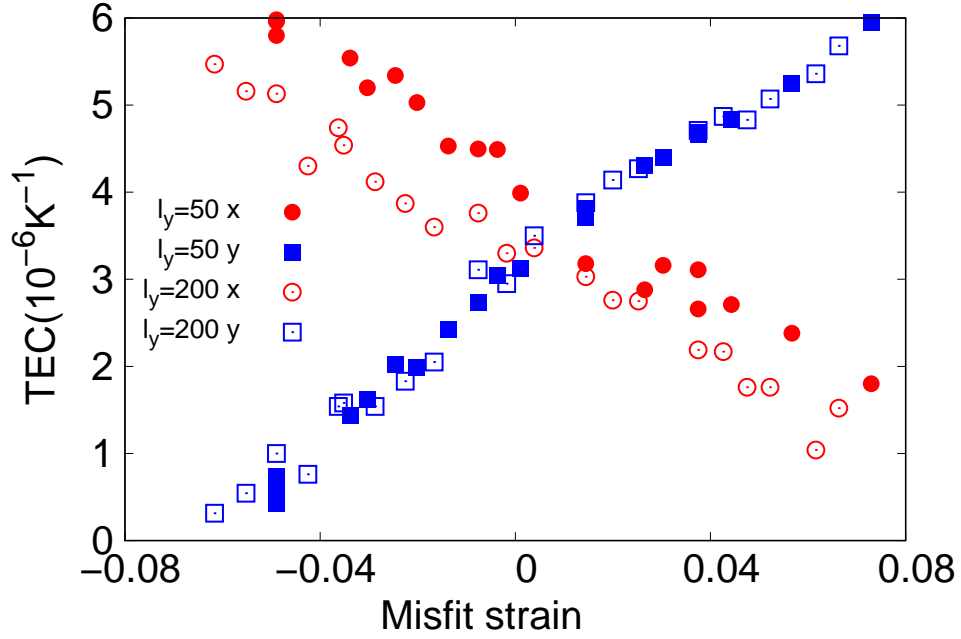


FIG. 4: TEC for graphene/MoS₂ heterostructures with varying misfit strains.

ripple effect is to reduce the TEC. It should be noted that the thermal induced ripple has an intrinsic length around 30-60 Å in graphene.⁴⁴ In graphene/graphene structures with dimension less than the intrinsic size, the thermal induced ripple is weakened due to the size confinement, so the negative effect from the ripple is weaker in smaller structures. Actually, Fig.3 shows that the size effect becomes less important for larger graphene/graphene structures with size above 60 Å, which further confirms the ripple based mechanism for the size effect. Hence, the TEC decreases with the increase of size for the graphene/graphene structure. Similar arguments are also applicable for the size dependence for the TEC of MoS₂/MoS₂ structures.

From the above, we have learned that MoS₂/MoS₂ structure has larger TEC than the graphene/graphene structure, and the thermal induced ripple has a negative effect on TEC. We now study the TEC for graphene/MoS₂ heterostructures. Fig. 4 shows TEC for graphene/MoS₂ heterostructure structures with different misfit strain. Two sets of heterostructures with quite different dimensions are simulated here. In the first set of heterostructures, the length along the y-direction is 199.2 Å and 199.6 Å for graphene and MoS₂ layers, respectively. These sizes are properly chosen, so that the misfit strain in the y-direction is minimum. The length along the x-direction for the graphene and MoS₂ layer is in the range of [187, 213] Å, so that the misfit strain is within [-6.2%, 6.6%]. In the second set of heterostructures, the length along the y-direction is 49.2 Å and 49.9 Å for graphene and MoS₂ layers, respectively. The length along the x-direction for the graphene and MoS₂ layer is in a wide range of [50, 105] Å.

The results in Fig. 4 shows that the TEC can be linearly tuned from $1 \times 10^{-6} \text{ K}^{-1}$ to $6 \times 10^{-6} \text{ K}^{-1}$ by the misfit strain. More specifically, the TEC along the x-direction decreases linearly with increasing misfit strain, while the TEC along the y-direction increases linearly with the increase of the misfit strain. The effect of the misfit strain is quite robust, as similar phenomenon can be observed for both sets of heterostructures with quite different lateral dimensions.

B. Misfit strain effect

To reveal the underlying mechanism for the misfit strain effect, we derive an analytic formula for the relation between the TEC and the misfit strain. The total strain energy of

a heterostructure related to the misfit strain is

$$U = \frac{1}{2}E_1\epsilon_1^2 + \frac{1}{2}E_2\epsilon_2^2, \quad (3)$$

where $\epsilon_1 = \frac{l-l_1}{l_1}$ and $\epsilon_2 = \frac{l-l_2}{l_2}$ are the strain for graphene and MoS₂ layers, respectively. Here l_1 and l_2 are the original lengths for graphene and MoS₂ layers, respectively. The l is the final length of the heterostructure structure after relaxation of the misfit strain. The E_1 and E_2 are the in-plane Young's moduli of graphene and MoS₂ layers, respectively. The final length l can be obtained by minimizing the total strain energy with respect to l ,

$$l = \frac{E_1 l_2 + E_2 l_1}{E_1 \frac{l_2}{l_1} + E_2 \frac{l_1}{l_2}}. \quad (4)$$

For a given temperature increasement of ΔT , the graphene and MoS₂ layers are expanded to $l'_1 = l_1(1 + \alpha_1 \Delta T)$ and $l'_2 = l_2(1 + \alpha_2 \Delta T)$, respectively, where α_1 and α_2 are the TEC of graphene and MoS₂ layers. The length for the heterosructure is,

$$l' = \frac{E_1 l_2 (1 + \alpha_2 \Delta T) + E_2 l_1 (1 + \alpha_1 \Delta T)}{E_1 \frac{l_2 (1 + \alpha_2 \Delta T)}{l_1 (1 + \alpha_1 \Delta T)} + E_2 \frac{l_1 (1 + \alpha_1 \Delta T)}{l_2 (1 + \alpha_2 \Delta T)}}. \quad (5)$$

With the definition of TEC, $\alpha = \frac{l'-l}{l\Delta T}$, the following analytic expression is obtained for the TEC of graphene/MoS₂ van der Waals heterostructrues,

$$\alpha = \frac{3E_1 E_2 (\alpha_1 - \alpha_2)}{(E_1 + E_2)^2} \epsilon_m + \frac{\alpha_1 E_1 + \alpha_2 E_2}{E_1 + E_2}. \quad (6)$$

Using the value of the Young's modulus and the TEC for graphene and MoS₂, we obtain the explicit relation between the TEC (in the unit of 10^{-6} K^{-1}) and misfit strain for the graphene/MoS₂ heterostructure

$$\alpha = -3.65\epsilon_m + 3.22. \quad (7)$$

This equation shows that the TEC is about $3.22 \times 10^{-6} \text{ K}^{-1}$ for the graphene/MoS₂ heterostructure without misfit strain, which agrees quite well with the MD simulation results. Furthermore, Eq. (7) shows that the TEC decreases linearly with the increase of misfit strain in the graphene/MoS₂, which is qualitatively consistent with the MD results. However, the slope for the linear function is only -3.65, which is about one order smaller than the MD result of -37.5 in Fig.4. It implies that some important factors must have been lost in deriving Eq. (7).

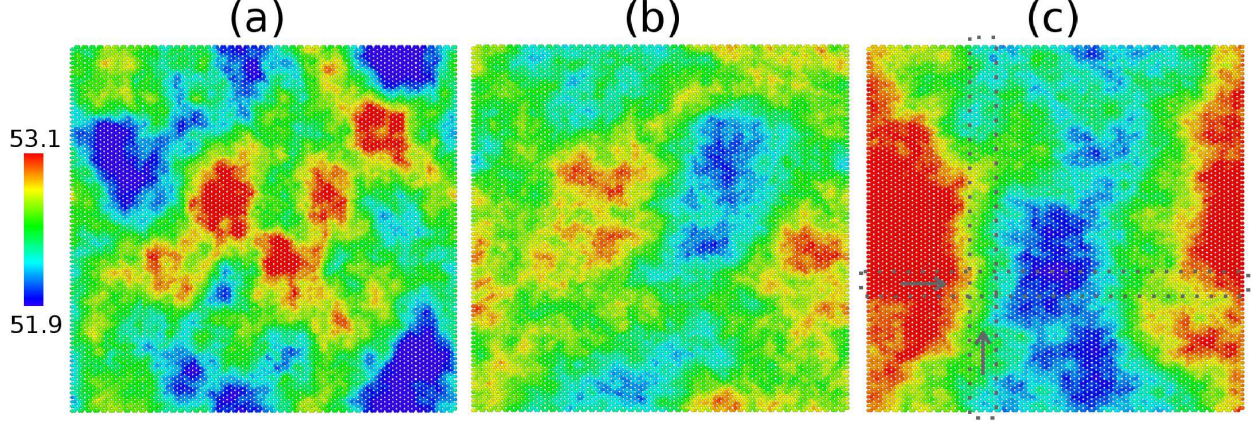


FIG. 5: The thermal induced ripples in graphene/MoS₂ van der Waals heterostructures with three typical misfit strains: (a) $\epsilon_m = -6.2\%$, (b) $\epsilon_m = 0.4\%$ and (c) $\epsilon_m = 6.2\%$. Color bar represents the z-coordinate of each atom.

C. Thermal induced ripple effect

It should be recalled that the thermal induced ripples play an important role in thermal and mechanical properties of the quasi-two-dimensional atomic layers like graphene/MoS₂ heterostructures. Particularly, the thermal induced ripple has negative effect on the TEC as shown in the above. Previous works have illustrated that the mechanical strain is an efficient way to tune the thermal induced ripples in atomic-layered structures^{45–48}. It is quite possible that the misfit strain (a specific mechanical strain) can affect the thermal induced ripples and may eventually influence the TEC of the graphene/MoS₂ heterostructure. We thus investigate the effect of the misfit on the thermal induced ripples in Fig. 5, where three quite different misfit strains are considered. The misfit strain is -6.2%, 0.4%, and 6.2% for these three structures. Obviously, the structure with large misfit strain in panel (c) has anisotropic ripples along the two in-plane directions, where the structure is slightly buckled along the horizontal x-direction.

The misfit strain effect on the ripples can be further quantified by introducing the effective thickness along the x and y directions, i.e., h_x and h_y . We take Fig. 5 (c) as an example to illustrate the definition and calculation of h_x . Scanning the figure from left to right along the horizontal x-direction, one gets the minimum and maximum value of the z-coordinate, i.e., z_{\min} and z_{\max} . The thickness along the x-direction is $h_x = z_{\max} - z_{\min}$. Similarly,

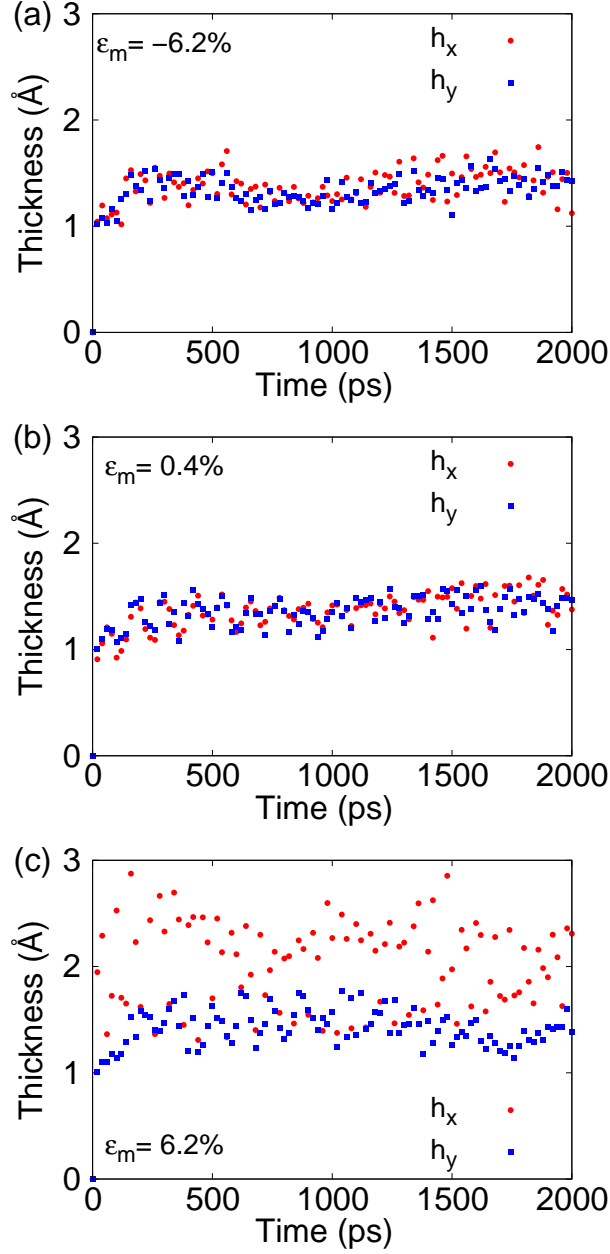


FIG. 6: The time history for the effective thickness of the graphene/MoS₂ with three typical misfit strains: (a) $\epsilon_m = -6.2\%$, (b) $\epsilon_m = 0.4\%$, and (c) $\epsilon_m = 6.2\%$. The temperature is 300 K.

h_y is calculated by scanning along the vertical y-direction. The thickness for Fig. 5 (c) is $h_x = 1.10$ Å and $h_y = 0.81$ Å. The effective thickness is anisotropic along these two in-plane directions, which truly represents the major feature of this structure.

Figure 6 shows the time history for the effective thickness at room temperature. Panels (a) and (b) show that the thickness is isotropic along the x and y directions for structures

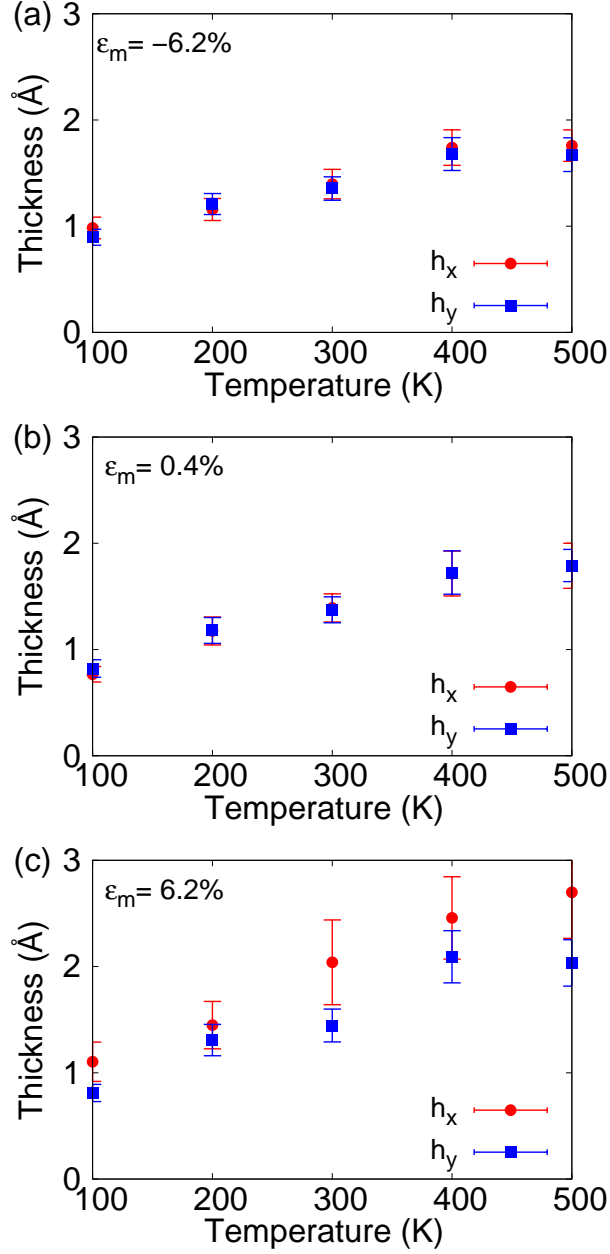


FIG. 7: The temperature dependence for the averaged effective thickness of the graphene/MoS₂ with three typical misfit strains: (a) $\epsilon_m = -6.2\%$, (b) $\epsilon_m = 0.4\%$, and (c) $\epsilon_m = 6.2\%$.

with $\epsilon_m = -6.2\%$ and 0.4% . Panel (c) shows that the graphene/MoS₂ heterostructure with large misfit strain of 6.2% has a large effective thickness along the x-direction. The effective thickness can be obtained by averaging over time. For example, we get $h_x = 1.10 \pm 0.18$ Å and $h_y = 0.81 \pm 0.08$ Å for the structure in Fig. 5 (c), where the error bar is the standard deviation error in the average over time.

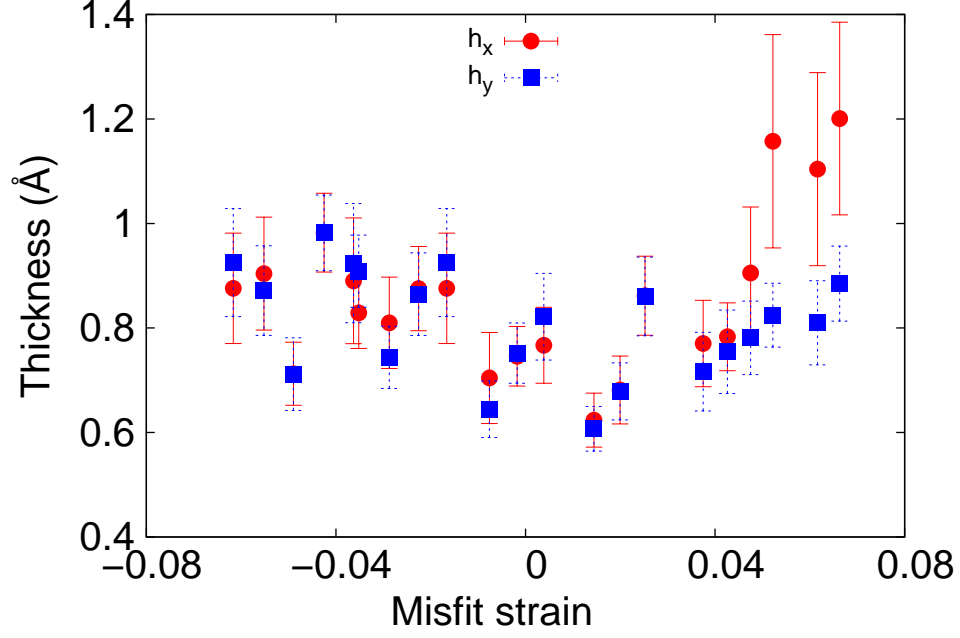


FIG. 8: The effective thickness for the graphene/MoS₂ heterostructure of different misfit strain at 100 K.

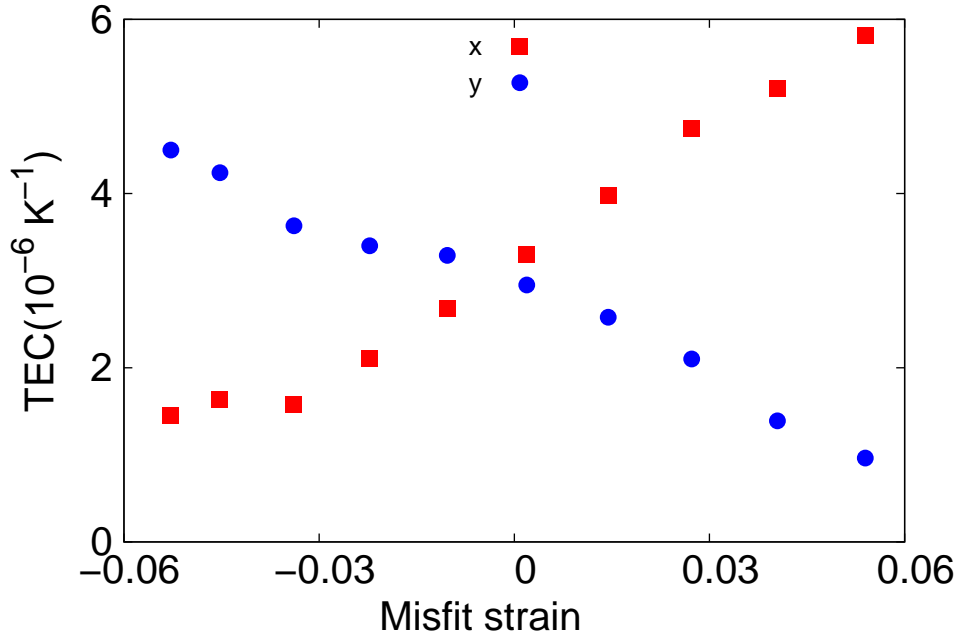


FIG. 9: The TEC for graphene/MoS₂ heterostructure with varying misfit strain along the y-direction. The misfit strain along the x-direction is almost zero (-0.2%).

The temperature dependence for the effective thickness is shown in Fig. 7 for these three graphene/MoS₂ heterostructures with different misfit strain. Panel (c) shows that the effective thickness is anisotropic in the structure with large misfit strain of 6.2%. Fig. 8 further illustrates that the effective thickness is anisotropic for structures with the misfit strain above 4%, where h_x is obviously larger than h_y . It is because the graphene layer is stretched while the MoS₂ layer is compressed by the misfit strain in the graphene/MoS₂ heterostructure with positive misfit strain. The MoS₂ layer is seriously compressed and will be slightly buckled as intrigued by the thermal vibration. The buckling of the MoS₂ layer will lead to the buckling of the whole heterostructure, as the graphene layer is much softer than the MoS₂ layer. The large thermal induced ripple along the x-direction causes a strong reduction of the TEC along the x-direction, leading to the decrease of the TEC along the x-direction with the increase of the misfit strain in Fig. 4. In contrast, the buckling along the x-direction can weaken the thermal induced ripples along the y-direction, so the y-directional TEC increases with increasing misfit strain. We have thus explained misfit strain effect on the TEC for $\epsilon_m > 0$ based on the thermal induced ripples.

For $\epsilon_m < 0$, the graphene layer is compressed while the MoS₂ layer is stretched by the misfit strain. Although the graphene layer is compressed seriously, the whole heterostructure is not buckled as can be seen from Fig. 5 (a), Fig. 6 (a), and Fig. 7 (a). The situation becomes more complex, as several competing mechanisms co-exist. On the one hand, the compressive misfit strain on the graphene layer tries to reduce the TEC along the x-direction, because compression can induce ripples that have negative effect on TEC. On the other hand, the positive misfit strain on the MoS₂ layer tries to increase the TEC along the x-direction, because the nonlinear effect becomes stronger upon stretching. The nonlinear effect will enhance the TEC. Our MD results show that the second mechanism surpasses the first mechanism, so the TEC along the x-direction increases with decreasing misfit strain for $\epsilon_m < 0$. One possible reason is that the TEC for MoS₂ is much larger than the TEC for graphene as can be seen from Fig. 3, so the second mechanism (on MoS₂) is more important than the first mechanism (on graphene).

In all above graphene/MoS₂ heterostructures, the misfit strain is almost zero along the y-direction, while the misfit strain in the x-direction is changed to tune the TEC. Fig. 9 shows similar misfit strain effect on the TEC in graphene/MoS₂ heterostructures with varying misfit strain along the y-direction.

IV. CONCLUSION

To summarize, the present work studies the effect of the misfit strain on the TEC of the graphene/MoS₂ heterostructure by MD simulations. The TEC can be tuned in a wide range from $1 \times 10^{-6} \text{ K}^{-1}$ to $6 \times 10^{-6} \text{ K}^{-1}$ by the misfit strain, and this misfit strain effect is not sensitive to the size or direction of the heterostructure. More specifically, the TEC along the misfit strain direction decreases linearly with the increase of misfit strain. Several possible underlying mechanisms are explored to be responsible for the misfit strain effect on the TEC. We first derive an analytic formula to directly relate TEC to the misfit strain, which qualitatively agrees with the MD results, but this analytic formula underestimates the misfit strain effect. We further demonstrate that the thermal induced ripples can be tuned by the misfit strain, which in turn causes strong effects on the TEC of the heterostructure. These results provide an effective manner to manipulate the TEC of van der Waals heterostructures through the misfit strain engineering.

Acknowledgment The work is supported by the National Natural Science Foundation of China (Grant Nos. 11822206 and 12072182) and Innovation Program of the Shanghai Municipal Education Commission (Grant No. 2017-01-07-00-09-E00019).

* Corresponding author: jwjiang5918@hotmail.com

¹ A. K. Geim and K. S. Novoselov, Nature Materials **6**, 183 (2007).

² A. A. Balandin, Nature Materials **10**, 569 (2011).

³ C. Lee, X. Wei, J. W. Kysar, and J. Hone, Science **321**, 385 (2008).

⁴ Y. Liu, N. O. Weiss, X. Duan, H. C. Cheng, and X. Duan, Nature Reviews Materials **1**, 16042 (2016).

⁵ Sobhit, Singh, Camilo, Espejo, Aldo, H., and Romero, Physical Review B **98**, 155309 (2018).

⁶ A. A. Balandin, S. Ghosh, W. Bao, I. Calizo, D. Teweldebrhan, F. Miao, and C. N. Lau, Nano Letters **8**, 902 (2008).

⁷ W. J. Yu, Q. A. Vu, H. Oh, H. G. Nam, H. Zhou, S. Cha, J. Y. Kim, A. Ca Rvalho, M. Jeong, and H. Choi, Nature Communications **7**, 13278 (2016).

⁸ Y. Zhong, G. Liu, J. M. Khan, and A. A. Balandin, Nature Communications **3**, 827 (2012).

- ⁹ Q. Liu, B. Cook, M. Gong, Y. Gong, D. Ewing, M. Casper, A. Stramel, and J. Wu, *Acs Applied Materials and Interfaces* **9**, 12728 (2017).
- ¹⁰ R. Frisenda, E. Navarro-Moratalla, P. Gant, D. P. D. Lara, P. Jarillo-Herrero, R. V. Gorbachev, and A. Castellanos-Gomez, *Chemical Society Reviews* **47**, 53 (2018).
- ¹¹ L. Chen, X. Li, C. Huang, S. Hu, and W. Han, *Journal of Materials Chemistry C* **8**, 4021 (2020).
- ¹² C. Wu, G. Zhao, Y. Xianbo, C. Liu, P. Lyu, G. Maurin, L. S., S. K., and N. Zhang, *Chemical Engineering Journal* **412**, 128736 (2021).
- ¹³ Q. H. Wang, K. Kalantar-Zadeh, A. Kis, J. N. Coleman, and M. S. Strano, *Nature Nanotechnology* **7**, 699 (2012).
- ¹⁴ L. Britnell, R. Gorbachev, R. Jalil, B. Belle, F. Schedin, A. Mishchenko, T. Georgiou, M. Katsnelson, L. Eaves, S. Morozov, et al., *Science* **335**, 947 (2012).
- ¹⁵ N. Mounet and N. Marzari, *Physical Review B* **71**, 205214 (2005).
- ¹⁶ K. V. Zakharchenko, M. I. Katsnelson, and A. Fasolino, *Physical Review Letters* **102**, 046808 (2009).
- ¹⁷ M. Pozzo, D. Alfe, P. Lacovig, P. Hofmann, S. Lizzit, and A. Baraldi, *Physical Review Letters* **106**, 135501 (2011).
- ¹⁸ S. Mann, R. Kumar, and V. K. Jindal, *Rsc Advances* **7**, 22378 (2017).
- ¹⁹ P. Anees, M. C. Valsakumar, and B. K. Panigrahi, *Physical Chemistry Chemical Physics* **19**, 10518 (2017).
- ²⁰ F. H. Liang, L. G. Peng, and Z. Zhi, *Physical Review B* **90**, 045409 (2014).
- ²¹ G. López-Polín, M. Ortega, J. Vilhena, I. Alda, J. Gomez-Herrero, P. Serena, C. Navarro, and R. Pérez, *Carbon* **116**, 670 (2017).
- ²² D. Yoon, Y. W. Son, and H. Cheong, *Nano Letters* **11**, 3227 (2011).
- ²³ G. A. McQuade, A. S. Plaut, A. Usher, and J. Martin, *Applied Physics Letters* **118**, 203101 (2021).
- ²⁴ L. Zhang, Z. Lu, Y. Song, L. Zhao, B. Bhatia, K. R. Bagnall, and E. N. Wang, *Nano Letters* **19**, 4745 (2019).
- ²⁵ G. Anemone, A. Al Taleb, A. Castellanos-Gomez, and D. Farias, *2D Materials* **5**, 035015 (2018).
- ²⁶ Z. Lin, W. Liu, S. Tian, K. Zhu, and Y. Yang, *Scientific Reports* **11**, 7037 (2021).
- ²⁷ K. H. Michel, S. Costamagna, and F. M. Peeters, *Physica Status Solidi* **252**, 2433 (2015).
- ²⁸ W. Bao, F. Miao, Z. Chen, H. Zhang, W. Jang, C. Dames, and C. N. Lau, *Nature Nanotechnology*

- nology **4**, 562 (2009).
- ²⁹ J. W. Jiang and H. S. Park, Applied Physics Letters **105**, 033108 (2014).
 - ³⁰ Y. C. Lin, C. Y. Chang, R. K. Ghosh, J. Li, H. Zhu, R. Addou, B. Diaconescu, T. Ohta, X. Peng, N. Lu, et al., Nano Letters **14**, 6936–6941 (2014).
 - ³¹ L. Y. Li and M. W. Zhao, Journal of Physical Chemistry C **118**, 19129 (2014).
 - ³² Z. H. Ni, W. Chen, X. F. Fan, J. L. Kuo, and Z. X. Shen, Physical Review B **77**, 115416 (2008).
 - ³³ J. Chaste, A. Missaoui, A. Saadani, D. G. Sanchez, and A. Ouerghi, ACS Applied Nano Materials **1**, 6752 (2018).
 - ³⁴ S. Shivaraman, J. Jobst, D. Waldmann, H. B. Weber, and M. G. Spencer, Physical Review B **87**, 195425 (2013).
 - ³⁵ J. D. He and J. W. Jiang, Nanotechnology **30**, 265701 (2019).
 - ³⁶ D. W. Brenner, O. A. Shenderova, J. A. Harrison, S. J. Stuart, B. Ni, and S. B. Sinnott, Journal of Physics:Condensed Matter **14**, 783 (2002).
 - ³⁷ F. H. Stillinger and T. A. Weber, Physical Review B **31**, 5262 (1985).
 - ³⁸ J. W. Jiang, Acta Mechanica Solida Sinica **32**, 17 (2019).
 - ³⁹ J. W. Jiang and H. S. Park, Journal of Applied Physics **117**, 124304 (2015).
 - ⁴⁰ S. Plimpton, Journal of Computational Physics **117**, 1 (1995).
 - ⁴¹ A. Stukowski, Modelling and Simulation in Materials Science and Engineering **18**, 015012 (2009).
 - ⁴² K. V. Zakharchenko, J. H. Los, M. I. Katsnelson, and A. Fasolino, Physical Review B **81**, 235439 (2010).
 - ⁴³ Z. Y. Wang, Y. L. Zhou, X. Q. Wang, F. Wang, Q. Sun, Z. X. Guo, and Y. Jia, Chinese Physics B **24**, 026501 (2015).
 - ⁴⁴ P. Gallagher, M. Lee, F. Amet, P. Maksymovych, J. Wang, S. Wang, X. Lu, G. Zhang, K. Watanabe, and T. Taniguchi, Nature Communications **7**, 10745 (2016).
 - ⁴⁵ S. Hussain, A. Liaqat, and M. A. Iqbal, Applied Physics Letters **117**, 153102 (2020).
 - ⁴⁶ J. Wang, R. R. Namburu, M. Dubey, and A. M. Dongare, Scientific Reports **7**, 40862 (2017).
 - ⁴⁷ L. Kou, Y. Ma, S. C. Smith, and C. Chen, Journal of Physical Chemistry Letters **6**, 1509 (2015).
 - ⁴⁸ F. Abualnaja, M. Hildebrand, and N. M. Harrison, Computational Materials Science **173**, 109422 (2020).